L.I.N.K.: optically aligned HUD-enabled rangefinding binoculars for wireless waypoint mapping

Brian Corchuelo, Dylan Farnsworth, Santiago Castro, and Jeremy Goodenough

College of Engineering and Computer Science and CREOL, The College of Optics and Photonics, University of Central Florida, Orlando, Florida 32816, USA

ABSTRACT

L.I.N.K. is a handheld optoelectronic binocular system that converts a visually selected distant target into a georeferenced map waypoint. The prototype combines a Keplerian binocular architecture, Porro-prism image erection, an optically injected heads-up display (HUD), a 905 nm time-of-flight laser rangefinder, inertial attitude sensing, global navigation satellite system (GNSS) positioning, and Bluetooth Low Energy (BLE) transfer to a phone-based mapping application. The optical design targets approximately 5× magnification, a 40 mm entrance pupil, a 4.5° true field of view, and a HUD image presented near optical infinity. One barrel contains a partially reflective combiner and display channel while the second remains an unobstructed viewing path. A tip-tilt LiDAR mount is used to register the ranging axis to the HUD reticle and binocular line of sight. The full senior design record documents completed embedded bring-up and sensor tests, including I^2C bus validation, BLE advertising, open-sky GNSS accuracy of approximately 3 m to 5 m, and calibrated BNO055 heading performance of approximately ±2°. Quantitative final optical, long-range LiDAR, and end-to-end waypoint tests remain incomplete and are explicitly identified rather than inferred.

Keywords: binocular optics, heads-up display, LiDAR, laser rangefinding, Porro prism, optical alignment, GNSS, waypoint mapping

1. INTRODUCTION AND SYSTEM REQUIREMENTS

Conventional mobile maps identify where the user is standing, but not necessarily the coordinate of a remote object that the user can see. L.I.N.K. addresses this limitation for hiking, field surveying, search planning, and landmark documentation. The operator observes a target through the binocular, centers the HUD reticle, acquires a laser range, and holds the acquisition control. The embedded unit captures the observer coordinate, heading, pitch, range, and supporting sensor state; computes the target coordinate; and transfers a waypoint to a progressive web application (PWA). The phone stores the pin locally, renders it on a map, and synchronizes it to a Node/Express and SQLite backend when a network is available.

The principal design risk is not the destination-point equation alone, but registration of the complete line-of-sight chain. The target seen by the eye, the reticle presented by the HUD, and the object sampled by the LiDAR must correspond. Accordingly, this paper emphasizes the optical barrels, display injection, LiDAR boresight, and their verification before summarizing the electronics and software.

Table 1. Optics-centered L.I.N.K. requirements extracted from the senior design specification.

Parameter	Requirement / design value	Role in system performance
Magnification	6× minimum / greater than 5× design goal	Resolves distant landmarks while remaining usable as a handheld instrument.
True / apparent field	4.5° / 22.5° optical-design target	Balances angular detail with situational awareness; the requirements table separately lists 20° AFOV.
Entrance pupil	40 mm	Establishes light collection and nominal exit-pupil scale.
Eye relief	20 mm	Supports comfortable observation, including use with eyeglasses.
LiDAR boresight	less than 1°	Limits cross-range displacement between the reticle and sampled target.
HUD latency	no more than 50 ms	Keeps status and acquisition feedback responsive.
LiDAR operating range	up to 200 m project requirement	Defines the intended field-validation envelope despite a larger vendor-rated module range.
Range / mapping error	±2 m / ±10 m targets	Combines range, GNSS, heading, boresight, and user-motion effects.
Package / mass	200 × 200 × 100 mm; less than 1500 g	Constrains the folded optical path and subsystem packaging.
Power	no more than 3.32 W; at least 1 h runtime	Sets battery, regulator, and LiDAR duty-cycle requirements.

FILL IN STILL: Reconcile the final measured magnification and AFOV with the conflicting 5×/20° requirements table and the greater-than-5×/22.5° optical-design text.

2. BINOCULAR OPTICAL DESIGN

2.1 Architecture and paraxial design

A Keplerian telescope was selected over Galilean and Newtonian alternatives because it provides an accessible real intermediate image and a wider field while remaining compatible with a compact binocular package. The objective forms an inverted real image; a Porro-prism pair erects the image and folds the optical path; and a positive eyepiece returns the output to an approximately afocal state. This architecture also provides a location for field conditioning and display injection that is not naturally available in a Galilean telescope. Standard geometrical-optics and binocular-design methods were used to establish the first-order layout.[1, 2, 3, 4]

For an elementary Keplerian system, the angular magnification is

$$M \approx -\frac{f_{\mathrm{obj,eff}}}{f_{\mathrm{eye}}}, \tag{1}$$

and the apparent field is approximately AFOV $\approx |M|$ TFOV. The paraxial Zemax model used a 160 mm focal-length, 40 mm diameter objective and a 40 mm focal-length, 25 mm diameter eyepiece. The selected off-the-shelf design subsequently replaced the eyepiece with a 50 mm component and inserted a negative focus extender, so the final magnification must be obtained from the complete ray trace rather than from the bare objective-to-eyepiece ratio.

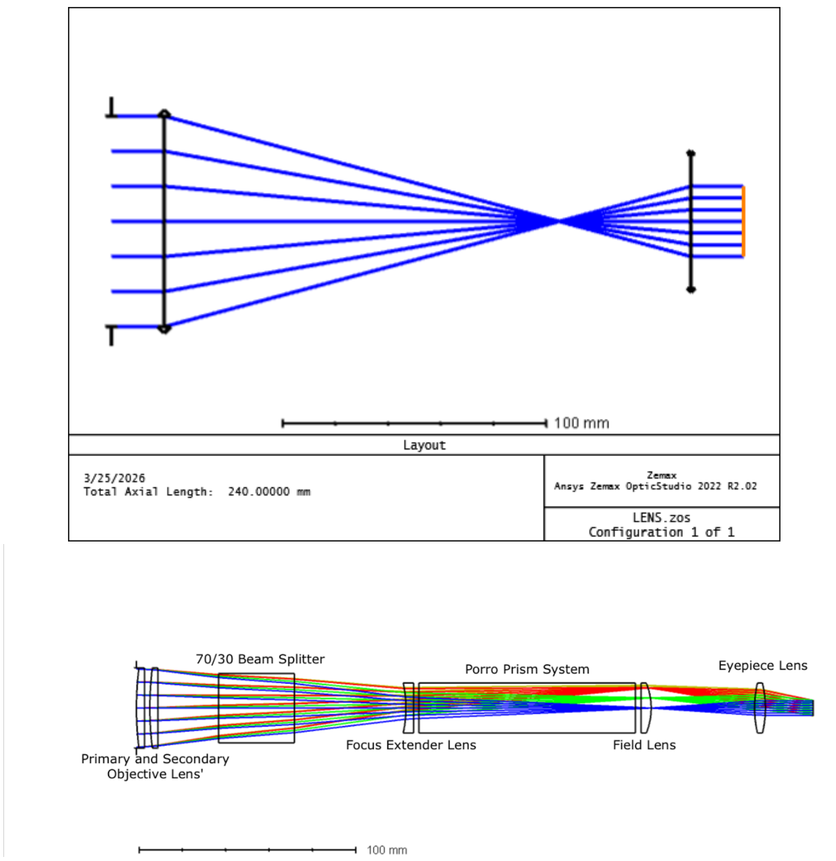

Figure 1. Top: Initial paraxial approximation. Bottom: Final, beam splitter Zemax view.

2.2 Off-the-shelf optical prescription

The final documented component set is summarized in Table 2. The achromatic objective reduces longitudinal color relative to a singlet and supplies the 40 mm entrance aperture. A −100 mm plano-concave focus extender moves the intermediate focus beyond the Porro assembly, allowing a positive field lens to be used after the prism folds. The field lens redirects off-axis bundles toward the eyepiece pupil and reduces vignetting. Both barrels use the same imaging train; the HUD barrel adds a combiner and a curved relay/fold mirror.

Table 2. Editable optical component summary for one L.I.N.K. barrel.

Element	Nominal focal length / ratio	Diameter / size	Function
Achromatic objective	160 mm	40 mm	Collects scene light and forms the initial real image with reduced chromatic aberration.
Focus extender	−100 mm	20 mm	Moves the intermediate focus outside the Porro assembly and modifies effective system power.
Porro prism pair	zero paraxial power	25 mm face class	Erects the image and folds the optical path into a compact binocular geometry.
Field lens	60 mm	25 mm	Controls the field bundles, pupil placement, and edge illumination.
Beam splitter	70:30 documented	20 mm documented	Transmits the scene and reflects the OLED image into the HUD barrel.
Eyepiece	50 mm	25 mm	Magnifies the intermediate image and collimates the output for the observer.

Table 3. Final optical results that are not numerically reported in the source document.

Metric	Final value	Evidence to insert
Magnification, AFOV	6X, 20 Degrees	Final Zemax chief-ray result and calibrated target measurement.
Exit pupil and eye relief	42mm, 18mm	Pupil analysis and physical pupil-camera or card measurement.
RMS spot / wavefront error	1.6 - 2.6um RMS Radius	Polychromatic plots for on-axis and edge-field points in both barrels.
Distortion and lateral color	2 mr	Grid-distortion and chromatic ray-fan/spot results.

The Porro pair provides two reflections in each prism, restoring the orientation of the Keplerian image while reducing the physical barrel length. The wider objective spacing also increases stereo baseline, although the primary waypoint computation uses range and heading rather than binocular stereopsis. Alignment of each prism is mechanically significant: wedge, tilt, or decenter produces image displacement and vertical disparity that the observer may be unable to fuse.

2.3 Zemax optimization and barrel matching

The report includes separate sequential models for Barrel 1 without the combiner and Barrel 2 with the HUD optics. Spot diagrams and ray-fan plots were generated at multiple field angles, and simulated images were compared with the paraxial image. The design record states that adding the off-the-shelf elements increased accessible field angle and improved aberration control, and that the two barrels had near-identical aberration, power, and field profiles after optimization. However, numerical RMS spot size, wavefront error, distortion, MTF, and relative illumination were not tabulated.

2.4 Focus, optomechanics, and verification method

The optical mounts were designed as separate objective, focus-extender/field-lens, Porro-prism, and eyepiece cells and assembled in a cage demonstration before the final enclosure. The advanced objective calls for manual focus from approximately 5 m to infinity. In the HUD barrel, the OLED, combiner/relay, and eyepiece should preserve their relative conjugate while the scene focus is adjusted; otherwise the user may obtain a sharp scene but a blurred overlay.

Magnification is planned to be measured by operating the telescope in reverse as a beam expander and comparing input and output beam diameters. The true field is measured from a known visible width W at distance D,

$$\theta_{\mathrm{TFOV}} = 2\tan^{-1}\left(\frac{W}{2D}\right), \quad (2)$$

with AFOV obtained from $|M|\theta_{\mathrm{TFOV}}$. Wavefront quality is planned to be measured at 633 nm using a Zygo interferometer and a return flat, separately for both barrels so that combiner-induced power, astigmatism, coma, and spherical aberration can be isolated.[5]

3. HUD OPTICAL INJECTION AND USER DISPLAY

The HUD uses a high-contrast emissive display so that inactive pixels add little stray background to the scene. The full design document selects a monochrome SSD1306-based 128×64 OLED connected by I^2C at address 0x3C.[6] Its documented pages show heading/pitch, GNSS status, barometric altitude/pressure, LiDAR range/quality, and BLE/queue state. A rotary encoder advances pages and a 2.5 s long press initiates waypoint capture. The report also proposes two linear polarizers, one

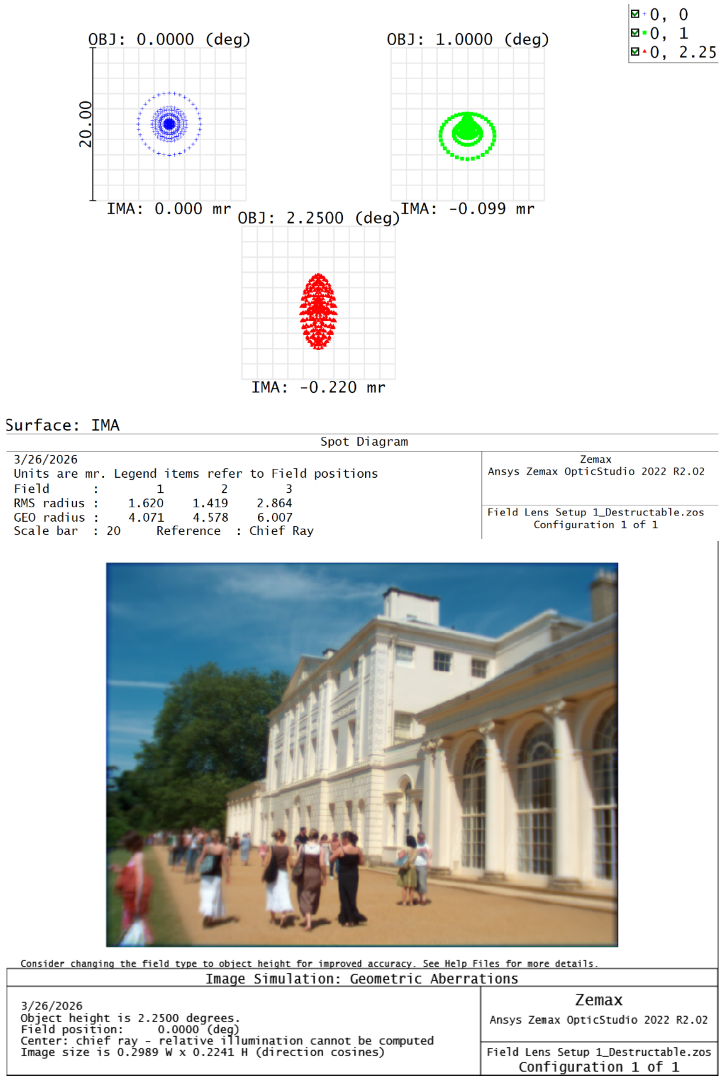

Figure 2. Top: Spot diagrams. Bottom: Simulated image.

Table 4. Measured mechanical adjustment ranges of the L.I.N.K. binocular assembly.

Parameter	**Measured value**	**Measurement definition**
Focus travel	**10** mm	Total axial displacement available to the eyepiece focusing assembly.
Interpupillary distance	**55–70** mm	Minimum-to-maximum center-to-center separation between the two optical barrels.

fixed and one rotatable, as a fully analog HUD brightness control.

The display path is described as a one-focal-length relay through the eyepiece. For an ideal thin lens,

$$\frac{1}{f} = \frac{1}{s} + \frac{1}{s'}, \tag{3}$$

and placement of the OLED at $s = f$ produces $s' \to \infty$. The eye therefore receives approximately collimated display light and can view the overlay without changing accommodation from a distant target. A partially reflective 70:30 combiner superimposes the reflected HUD channel on the transmitted scene. The combiner ratio is a practical compromise: increasing reflectance improves OLED visibility but reduces scene throughput. Ghost images, OLED pixel visibility, combiner wedge, field clipping, and eye-position parallax should be evaluated experimentally.

HUD readability testing is currently planned as a human-subject-style font-size comparison because the 128-by-64

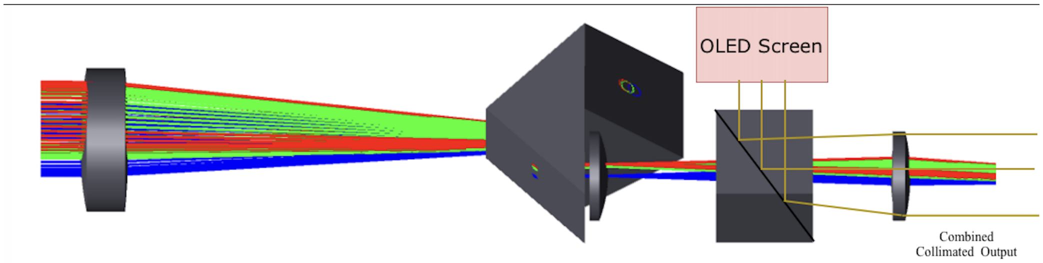

Figure 3. Further explanation of HUD system through Zemax.

display and near-unity relay magnification limit usable character size. Participants will rank candidate font sizes for comfort and legibility. Additional quantitative tests should measure display luminance, scene transmission, virtual-image distance, eyebox dimensions, and parallax while the eye moves across the usable pupil.

4. LIDAR RANGING, BORESIGHT, AND LASER SAFETY

4.1 Rangefinder selection and measurement model

Pulsed time-of-flight (ToF) ranging was selected over phase-shift and frequency-modulated continuous-wave approaches because it provides direct absolute range with lower cost and implementation complexity for stationary field targets.[7, 8] The distance is

$$R = \frac{c\Delta t}{2n}, \tag{4}$$

where Δt is the round-trip interval and n is the refractive index of the propagation medium. A commercial module performs the transmit, receive, timing, and internal averaging, leaving the microcontroller to validate and consume the reported range.

The selected long-range unit is identified as the PTYS-12X-251028: a 905 nm, 3.3 V, UART/TTL module measuring approximately $22.5 \times 16 \times 9.5$ mm and rated for −20 °C to 60 °C. The project document reports vendor maximum ranges of 1200 m by day and 2000 m by night and identifies the module as Class 1. Those values are vendor claims, not demonstrated L.I.N.K. performance; the project requirement limits the intended operating test to 200 m.

The testing chapter separately describes a TFMini-Plus-class bench module that produces 0x59 0x59 binary frames and is evaluated against the larger of ±5 cm or ±1%. This protocol and accuracy statement should not be assigned to the PTYS-12X until the final hardware is confirmed.

4.2 Boresight alignment

The LiDAR mount is designed with spring-loaded tip and tilt adjustment analogous to a mirror mount. A reticle is centered in the binocular field and the target is placed at the 50 m minimum working range. With the reticle centered on the target, an infrared camera locates the invisible 905 nm spot and the mount is adjusted until the spot is coincident with the reticle. The target is then moved outward in 50 m increments to verify that the axes remain parallel rather than merely crossing at one distance.

For small boresight error $\Delta\theta$, the cross-range miss is

$$E_{\perp} = R\tan(\Delta\theta) \approx R\Delta\theta. \tag{5}$$

The current less-than-1° requirement permits a 3.49 m cross-range error at 200 m; a tighter final tolerance may therefore be required to meet the 10 m total mapping-error objective after GNSS and IMU error are included.

4.3 Range verification and safety controls

The documented characterization procedure places a flat target at surveyed distances, records 100 consecutive readings at each location, and reports mean error, standard deviation, signal strength, and valid-return fraction. Range linearity should be repeated over target reflectance, incidence angle, ambient light, and weather. Final boresight should be reported in horizontal and vertical milliradians rather than only as a visual centered/not-centered judgment.

The LiDAR is treated under IEC 60825-1 laser classification.[9] Although the selected module is reported as Class 1, the wavelength is invisible and is used adjacent to binocular viewing optics. The proposed engineering and administrative controls are a manual shutter, an external laser-on indicator, a HUD warning, and an exterior classification label. The final assembly must preserve the module's certified accessible-emission condition; modification of apertures or optics can invalidate reliance on the original classification.

Table 5. Preliminary optical and navigation error-budget entries at 200 m.

Term	Documented value / target	Equivalent effect and required test
GNSS horizontal position	approximately 3 m to 5 m open sky	Direct translation of observer origin; repeat against surveyed control points.
IMU heading	approximately ±2° after calibration	Up to approximately 6.98 m cross-range at 200 m; repeat over azimuth and near final electronics.
LiDAR boresight	less than 1° requirement	Up to 3.49 m cross-range at 200 m; measure horizontal and vertical offset in mrad.
Range	±2 m project target	Primarily radial error; measure bias and repeatability over distance and reflectance.

5. OPTICAL ERROR BUDGET AND FIELD-VERIFICATION PLAN

The mapping requirement is a system-level quantity rather than a specification of any single sensor. A useful first-order decomposition separates radial error from cross-range error. Range uncertainty contributes mainly along the measured line of sight. GNSS error translates both the observer and target solution. Heading, LiDAR boresight, and HUD parallax produce angular error that is converted to cross-range displacement by target distance. For independent small errors, a preliminary planning expression is

$$\sigma_{\mathrm{map}}^2 \approx \sigma_{\mathrm{GNSS}}^2 + \sigma_R^2 + R^2\left(\sigma_{\theta,\mathrm{IMU}}^2 + \sigma_{\theta,\mathrm{bore}}^2 + \sigma_{\theta,\mathrm{HUD}}^2 + \sigma_{\theta,\mathrm{motion}}^2\right), \tag{6}$$

where angular terms are expressed in radians. Equation (6) is not a substitute for measured covariance, but it shows which quantities must be recorded during field tests.

The measured open-sky GNSS error in the report is approximately 3 m to 5 m, and the calibrated BNO055 heading result is approximately ±2°. At 200 m, a 2° heading error alone corresponds to approximately 6.98 m cross-range displacement. The less-than-1° boresight requirement permits up to 3.49 m at the same range. These values indicate that the 10 m mapping objective is plausible only when the heading and boresight errors are near their better operating values and the user holds the instrument steadily. This conclusion is an error-budget inference from the documented subsystem values, not an end-to-end measurement.

The recommended field campaign begins with barrel-level verification before the waypoint software is evaluated. First, measure magnification, field, exit pupil, eye relief, and transmitted wavefront for each barrel. Second, align the HUD reticle to the selected viewing axis and quantify parallax across the eyebox. Third, characterize the rangefinder independently using known distances and multiple target materials. Fourth, adjust LiDAR tip and tilt at 50 m and verify the angular offset at 100 m, 150 m, and 200 m. Finally, acquire repeated waypoints to pre-surveyed landmarks at multiple bearings. Each trial should preserve the raw observer coordinate, satellite count, HDOP, heading, pitch, IMU calibration scores, range, signal quality, reticle offset, target truth coordinate, and environmental conditions.

A minimum useful result set is three or more repeated acquisitions per target at several ranges and azimuths. Report mean radial error, cross-range error, total horizontal error, standard deviation, and failure rate. Separating radial and cross-range components allows a range bias to be distinguished from heading or boresight error. Repeating the test after transport and focus adjustment also determines whether the mechanical design maintains calibration, which is essential for a field instrument rather than a one-time laboratory alignment.

6. EMBEDDED ELECTRONICS AND WAYPOINT PIPELINE

6.1 Controller, sensor suite, and power

The tested embedded platform is an ESP32-S3-DevKitC-1 with a WROOM-2 N32R16V module, selected for integrated BLE and sufficient UART, I^2C, SPI, and GPIO resources.[10, 15] The shared 400 kHz I^2C bus uses GPIO 8/9 and includes the BNO055 IMU at 0x28, BMP280 at 0x76 or 0x77, and SSD1306 at 0x3C. The GNSS receiver uses UART2 at 9600 baud; the bench LiDAR uses a separate high-rate UART. During bring-up, all three I^2C addresses were detected and disappeared individually when disconnected, validating power, pull-ups, and the absence of address collisions.

The power system uses a single-cell lithium source and an LTC3113 buck-boost regulator producing 3.3 V.[11] The worst-case component estimate is 775.47 mA, dominated by the 450 mA LiDAR allocation. This corresponds to 2.559 W ideal rail power and approximately 2.843 W at 90% conversion efficiency. With a 3000 mA h cell, the analytical runtime is 3.91 h, exceeding the 1 h requirement but not yet replacing a measured load test.

Table 6. Major embedded functions and documented validation state.

Subsystem	Interface / rate	Documented role or result
ESP32-S3	GPIO, UART, I^2C, BLE	Booted, completed a 10 min soak, advertised as LINK-HUD, and streamed stub telemetry.
BNO055 IMU	I^2C, 20 Hz	Heading settled to about ±2° after calibration; pitch/roll agreed within about ±1°.
GT-U7 / NEO-7M-class GNSS	UART, 1 Hz NMEA	Open-sky cold start 30 s to 60 s, 8–12 satellites, approximately 3 m to 5 m horizontal accuracy.
BMP280	I^2C	Pressure/temperature/altitude with GPS-assisted sea-level-pressure calibration; final stability data not reported.
SSD1306 OLED / encoder	I^2C / GPIO	Five pages, one-detent page changes, 2.5 s long-press acquisition, 250 ms debounce.
LiDAR	UART	Bench frame parsing defined; final PTYS-12X outdoor characterization remains incomplete.

Table 7. Current verification status from the full senior design document.

Area	Documented evidence	Remaining evidence
Optical feasibility	Keplerian/Porro cage demonstration assembled; Zemax layouts, ray fans, spots, and simulated images produced.	Measured magnification, TFOV/AFOV, eye relief, distortion, resolution/MTF, and interferometry.
HUD	SSD1306 pages and encoder logic exercised electrically; infinity-conjugate concept modeled.	Integrated luminance, readability, parallax, eyebox, focus tracking, and outdoor visibility.
LiDAR	ToF architecture and final module selected; bench parser/test method documented.	Confirm final module; range linearity/repeatability, reflectance, outdoor maximum range, and boresight in mrad.
IMU	Heading about ±2°; pitch/roll about ±1° after calibration.	Repeatability, thermal drift, and magnetic-interference map in final enclosure.
GNSS	Open-sky 3 m to 5 m; degraded 8 m to 12 m; phone/device agreement 5 m to 10 m.	Larger sample, fixed truth points, and final antenna/enclosure effects.
BLE/PWA	Advertising and prototype map rendering partially demonstrated; retry architecture implemented in design.	Full packet/ACK test, offline queue test, latency, and duplicate prevention on final hardware.
End-to-end waypoint	Test procedure and error model defined.	Repeated known-landmark trials at multiple ranges and bearings with radial/cross-range statistics.

6.2 Firmware, coordinate computation, and communications

The firmware is a cooperative state machine with a 20 Hz sensor poll, 5 Hz BLE telemetry, a 2.5 s acquisition hold, a 10 s retry interval, and a 32-pin local queue. Each driver reports OK, DEGRADED, or FAIL. A ping is rejected when GNSS, IMU, or range data are invalid, while noncritical failures do not crash telemetry or the user interface.

Let observer latitude/longitude be (ϕ_1, λ_1), bearing be θ, range be d, Earth radius be R_E, and $\delta = d/R_E$. The destination is

$$\phi_2 = \sin^{-1}(\sin\phi_1 \cos\delta + \cos\phi_1 \sin\delta \cos\theta), \tag{7}$$

$$\lambda_2 = \lambda_1 + \tan^{-1}\left(\frac{\sin\theta \sin\delta \cos\phi_1}{\cos\delta - \sin\phi_1 \sin\phi_2}\right). \tag{8}$$

At these ranges, practical sensor and alignment errors exceed the spherical-Earth model error. Heading error creates approximately $E_h = R\sin\theta_{\text{error}}$ lateral displacement: a 1° error gives 4.36 m at 250 m and 8.73 m at 500 m.

The ESP32 exposes telemetry, pin, acknowledgment, and calibration characteristics through a custom BLE GATT service.[12] Telemetry and pin records are JSON.[13] The embedded queue retains a pin until the phone acknowledges it; the PWA then uses IndexedDB to retain the record until the Express/SQLite backend accepts it. This two-stage queue separates BLE recovery from network recovery and prevents one-time field observations from being silently lost.

7. VERIFICATION STATUS AND DISCUSSION

Table 7 distinguishes completed observations from planned tests. The full report contains meaningful embedded and GNSS results, but final optical, HUD, long-range LiDAR, and end-to-end waypoint data are not yet available. Expected waypoint accuracy of approximately 5 m to 10 m at short range and 10 m to 25 m at medium range is an engineering projection, not a measured result.

The dominant anticipated error terms are GNSS position, magnetic heading error, LiDAR range, LiDAR-to-reticle boresight, hand motion during the long press, and HUD parallax. Range error is primarily radial. Heading and boresight error are cross-range terms that grow linearly with target distance. Final reporting should therefore include the raw observer coordinate, satellite count/HDOP, IMU calibration state, range and signal quality, reticle offset, target truth coordinate, and repeated-trial statistics instead of only a single total-error number.

8. CONCLUSION

L.I.N.K. combines a two-barrel Keplerian/Porro binocular, an infinity-focused OLED HUD, a near-infrared ToF rangefinder, and embedded navigation sensors to produce map waypoints for visually selected distant targets. The full project documentation supports a substantially more detailed SPIE manuscript than the earlier conference draft: it defines the optical component train, HUD controller and pages, proposed LiDAR alignment fixture, laser-safety controls, power budget, firmware timing, sensor validation, and waypoint data pipeline. The remaining publication-critical work is quantitative. Final submission should replace every

ACKNOWLEDGEMENTS

The authors acknowledge Dr. Chung Chan, Dr. Lei Wei, Dr. Paul Leisher, Dr. Qifeng Li, Dr. Yannick Salamin, Dr. Darren Hudson, the University of Central Florida College of Engineering and Computer Science, CREOL, The College of Optics and Photonics, and Edmund Optics for support and sponsored optical components.

REFERENCES

[1] E. Hecht, *Optics*, Pearson (edition/year: FILL IN STILL).

[2] W. J. Smith, *Modern Optical Engineering*, McGraw-Hill (edition/year: FILL IN STILL).

[3] J. E. Greivenkamp, *Field Guide to Geometrical Optics*, SPIE Press, Bellingham, Washington (publication details: FILL IN STILL).

[4] R. Kingslake, *Lens Design Fundamentals* (edition/publisher/year: FILL IN STILL).

[5] D. Malacara, *Optical Shop Testing* (edition/publisher/year: FILL IN STILL).

[6] Solomon Systech, "SSD1306 OLED display controller," datasheet (revision/year: FILL IN STILL).

[7] M.-C. Amann, T. Bosch, M. Lescure, R. Myllylä, and M. Rioux, "Laser ranging: a critical review of usual techniques for distance measurement," *Optical Engineering* 40(1), 10–19 (2001).

[8] B. Schwarz, "LIDAR: mapping the world in 3D," *Nature Photonics* 4, 429–430 (2010).

[9] International Electrotechnical Commission, "IEC 60825-1: Safety of laser products," (edition/year used by project: 2014; confirm complete citation).

[10] Espressif Systems, "ESP32-S3 series datasheet," (revision/year: FILL IN STILL).

[11] Analog Devices, "LTC3113: 3 A low-noise buck-boost DC/DC converter," datasheet (revision/year: FILL IN STILL).

[12] Bluetooth Special Interest Group, "Bluetooth Core Specification 5.4" (2023).

[13] T. Bray, "The JavaScript Object Notation (JSON) Data Interchange Format," RFC 8259, Internet Engineering Task Force (2017).

[14] **FILL IN STILL:** Manufacturer, complete title, revision, date, and URL for the PTYS-12X-251028 905 nm rangefinder datasheet.

[15] Bosch Sensortec, "BNO055 intelligent 9-axis absolute orientation sensor," datasheet (revision/year: FILL IN STILL).